photonics

MDPI

Article

Characterization and Direct Modulation of a Multi-Section PIC Suited for Short Reach Optical Communication Systems

Mohab N. Hammad [1,*], Aleksandra Kaszubowska-Anandarajah [2], M. Deseada Gutierrez Pascual [3], Pascal Landais [1], Prajwal D. Lakshmijayasimha [1], Gaurav Jain [3] and Prince M. Anandarajah [1]

1 Photonics Systems and Sensing Lab., School of Electronic Engineering, Dublin City University, Glasnevin, 9 Dublin, Ireland; pascal.landais@dcu.ie (P.L.); prajwal.doddaballapural2@mail.dcu.ie (P.D.L.); prince.anandarajah@dcu.ie (P.M.A.)
2 CONNECT Research Centre, Dunlop Oriel House, Trinity College Dublin, 2 Dublin, Ireland; anandara@tcd.ie
3 Pilot Photonics, Invent Centre, Dublin City University, Glasnevin, 9 Dublin, Ireland; desi.gutierrez@pilotphotonics.com (M.D.G.P.); gaurav.jain@pilotphotonics.com (G.J.)
* Correspondence: mohab.hammad2@mail.dcu.ie

Received: 29 June 2020; Accepted: 28 July 2020; Published: 31 July 2020

Abstract: A multi-section active photonic integrated circuit (PIC) is characterized in detail to gauge its suitability as a transmitter for short reach applications. The PIC is 1.5 mm long and consists of two lasers integrated in a master-slave configuration, which enables optical injection locking (OIL) of the slave laser. The beneficial impact of the injection is characterized by static and dynamic measurements. The results show a reduction of the optical linewidth from 8 MHz to 2 MHz, a relative intensity noise (RIN) value as low as −154.3 dB/Hz and a 45% improvement of the slave laser modulation bandwidth from 9.5 GHz to 14 GHz. This frequency response enhancement allows the direct modulation of the slave gain section at a data rate of 10.7 Gb/s and an error-free transmission over 25 km of standard single-mode fiber (SSMF). Transmission performance of the injected case shows a 2 dB improvement in the minimum optical power required to achieve a bit error rate of 3.8×10^{-3} (hard decision forward error correction limit). These results demonstrate that the multi-section PIC can serve as an attractive cost-efficient transmitter in a wide variety of low-cost short-reach data communication applications.

Keywords: photonic integration; optical injection; linewidth; relative intensity noise (RIN); frequency response; direct modulation; bit error rate (BER)

1. Introduction

The ever increasing demand for bandwidth hungry applications, such as ultra-high definition video streaming, high resolution online video gaming and cloud services, are placing intensive pressure on existing fiber optic communication networks [1]. This has led to a "capacity crunch", where the existing networks struggle to meet the required bandwidth imposed by these new services and applications. Amongst the different network segments, the short reach and data centre networks (DCNs) form the last mile of the optical network. They require innovative low cost and low power solutions to be able to respond to the ever-increasing bandwidth demand challenges. Photonic integration [2] provides a promising alternative to systems employing discrete components. By integrating multiple optical functionalities onto one chip, photonic integration can deliver cheaper, lower footprint, and lower power consumption solutions for optical networks. This can be a major advantage for DCNs, where compactness, cost, and power efficiency are critical [3]. Photonic integrated circuits (PICs) are built from many different materials, on custom manufacturing platforms. These include silicon

(Si), silica (SiO2), lithium niobate (LiNbO3), silicon nitride (SiN), indium phosphide (InP), polymer, or glass [4]. PICs provide many attractive features, including smaller photonic dies, higher data rates, lower power consumption, lower cost per bit of data, and better reliability compared to legacy optics. Integrating multiple lasers in a single chip provides many advantages, such as the ability to achieve in-chip optical injection locking (OIL). OIL entails injecting light from a master laser into the cavity of a slave laser, thus transferring its frequency and phase to the slave laser [5]. The transfer of the spectral characteristics from a spectrally purer master to a slave laser allows the improvement of various characteristics of the slave laser, such as optical linewidth [6], relative intensity noise (RIN) [7], and mode partition noise (MPN) [8]. Furthermore, it can also enhance the laser modulation bandwidth [9] and resonance frequency [10]. Several studies have shown that the OIL can push the slave laser modulation bandwidth beyond the k-factor limit [11]. A discrete OIL setup comprises different passive and active optical components, such as circulators, polarization controllers, isolators, master, and slave lasers. Such a setup suffers from instabilities due to polarization dependence in case of usage of standard single mode fiber (SSMF). Use of polarization maintaining fiber (PMF) based components could avoid the polarization dependence issue. However, it still suffers from temperature variation in the injection path and introduce large insertion losses (due to the passive components used). An on-chip (integrated) OIL solution can provide the same advantages as a discrete OIL setup, whilst offering a simpler, cheaper, smaller footprint, and polarization independent operation.

From the DCN and access network perspective, the ability to increase the modulation bandwidth of a laser is of particular interest, as it enables direct modulation of commercially available lasers with higher data rates. Direct modulation is a simple modulation technique, where the amplitude of the optical wave is modified, by varying the strength of the laser excitation [12]. It alleviates the requirement for bulky and lossy external modulators in the transmitter, thus providing a cost and energy-efficient solution for DCNs. The high sensitivity of DCNs to both cost and energy favours direct modulation as an electro-optic conversion technique. Previous work has shown that multiple lasers implemented in a single PIC in a master-slave configuration can be directly modulated and used as a transmitter in short reach networks. In [13], the authors report on a two-section discrete mode laser device in a master-slave configuration that achieves a side mode suppression ratio (SMSR) over 50 dB and a RIN of −142.6 dB/Hz. The laser is then directly modulated at a bit rate of 10 Gb/s, delivering an error-free back to back (B2B) transmission at a received optical power of −11 dBm. Furthermore, the same laser reported in [13] was subsequently directly modulated and used to transmit a 10 Gb/s signal over 50 km of SSMF [14]. Such long-distance transmission is achieved due to the reduction of the direct modulation induced frequency chirp by implementing OIL [15]. Chirp, in systems employing direct modulation, is considered as one of the main limiting factors both in terms of the spectral efficiency as well as transmission distance (due to the interplay between the chirp and the fiber dispersion). The design of the chip in [14] can be further improved by introducing additional, grating sections to the device. This would allow the lasing frequency of each laser to be tuned separately, thus providing much better control over the emission wavelength. Moreover, it provides more control over the power injected from the master laser, allowing for the optimization of the OIL, thus optimizing the overall performance of the integrated device. Furthermore, dividing each laser into two different sections gives the ability to control the bias of each section individually. This results in achieving accurate control over the Bragg condition (accurate overlap between the longitudinal mode of the FP laser and the Bragg mirror reflection), hence better compensation of cleaving facets error.

In this paper, we present an Indium Phosphide (InP) PIC that comprises of four sections, with different cavity lengths, realized in a master-slave configuration. All the sections of the PIC are active and can be biased separately. The complexity of the device structure and the amount of combinations of biases for each section results in different regimes of operation. Hence, an extensive characterization of the device, under different bias conditions, is critical in order to comprehend the device behaviour. Thus, in this paper, we present a detailed analysis of the device performance, under several bias conditions. We first carry out a static characterization of the PIC-based transmitter.

The effect of injecting light from the master into the slave laser on vital transmitter parameters, such as linewidth and RIN, is presented. Subsequently, the dynamic characterization of the device, with and without injection from the master laser, is also presented and the enhancement of the PIC modulation bandwidth under OIL is shown. Finally, using the optimum operating conditions obtained from both static and dynamic characterizations, the performance of the PIC in a short reach network scenario is verified qualitatively and quantitatively through eye diagrams and BER as a function of the received optical power measurements.

The paper is organized as follows: Section 2 includes a full description of the PIC design and the specifications of the different sections. Section 3 presents the results of the static characterisation of the device, while the dynamic characterisation of the PIC is shown in Section 4. This includes a comparative study (with and without OIL) of the frequency response, as well as the validation of the device performance in a 10.7 Gb/s directly modulated transmission system. Finally, conclusions are drawn in Section 5.

2. Device Description

The schematic of the multi-section PIC is shown in Figure 1a. The device is fabricated using a standard 1550 nm laser material (InP). Five strained ($(Al_{0.23}Ga)_{0.3}In_{0.7}As$) quantum wells of 5 nm thickness form the active region. This active region is placed on an n-doped InP substrate. There are in total 22 slots with a depth of 1.395 µm, as shown in Figure 1b, which represents the side view of the device. These slots are used to control the longitudinal spectrum. Standard electron beam lithography is used in the fabrication of the slots to provide precise control of the slots' dimensions (width, depth) and location [16]. The total length of the device is ~1.5 mm. The PIC consists of two regrowth-free Fabry-Pérot (FP) lasers, integrated into a master-slave configuration. Each laser consists of two electrically isolated sections, with different cavity lengths named gain and reflector sections, as shown in Figure 1c. The gain section of each laser is a FP structure that generates and amplifies the light inside the cavity. This gain section has an anti-reflection (AR)-coated facet. Each of the multiple reflector sections of the laser serves as a grating. The multiple uniformly distributed slots in the reflector section act as a filter that enhances various FP mode(s), but suppresses other modes of the FP resonance. Hence, it restricts the FP laser to a single mode of the allowed FP cavity modes. This results in achieving a single longitudinal mode emission [17]. These distributed slots can be considered as an active distributed Bragg grating [18]. The left facet at the end of the slots region (reflector section) is high-reflection (HR)-coated. Both reflector sections of the two lasers are etched into the surface ridge waveguide, close to the active region, to provide internal reflections and enable a high SMSR (~50 dB) [16]. Furthermore, they provide improved control of the emission wavelength and the injection power inside the PIC. Both sections of the laser (gain and reflector) share the same active layer and InP substrate. Besides consisting of two main sections, which are the master reflector (MR) and the master gain (MG), the master laser shares the slave reflector (SR) with the slave laser, which enables a reduction of the overall length of the device, providing better confinement and control of the total temperature of the PIC. The length of each section is optimized for its specific functions which enable the optimization of the PIC as a device for employment in short reach networks. The master gain is designed to be the longest of all sections (712 µm), in order to achieve a low linewidth emission. The slave gain section, on the other hand, is much shorter (355 µm), to ensure a high modulation bandwidth. The two reflector sections have an equal length of 215 µm. The isolation between different sections is achieved by separating them with a 2 µm wide etched trench, whose impedance is measured to be 2.29 kΩ.

As the PIC consists of two distinct lasers, two independent spectral modes, corresponding to each laser, can be generated by the device. A continuous-wave (CW) spectrum of the master (biased at 35 mA) and slave (biased at 90 mA), operating in single-mode regime, is shown in Figure 2a (OSA resolution: 20 pm). Biasing the device at "bias point 1" listed in Table 1 results in achieving the injection locking spectrum shown in Figure 2b. To further confirm the independence of the two lasers, the two

independent spectral modes are shown again in Figure 2c, where the OSA is set to a finer resolution of 0.04 pm. The master laser and slave lasers are biased at 40 and 60 mA, respectively. OIL is achieved again at "bias point 2" listed in Table 1 and its spectrum is shown in Figure 2d. It is important to note that OIL could be achieved at several other bias points, but we only highlight the two listed points for brevity.

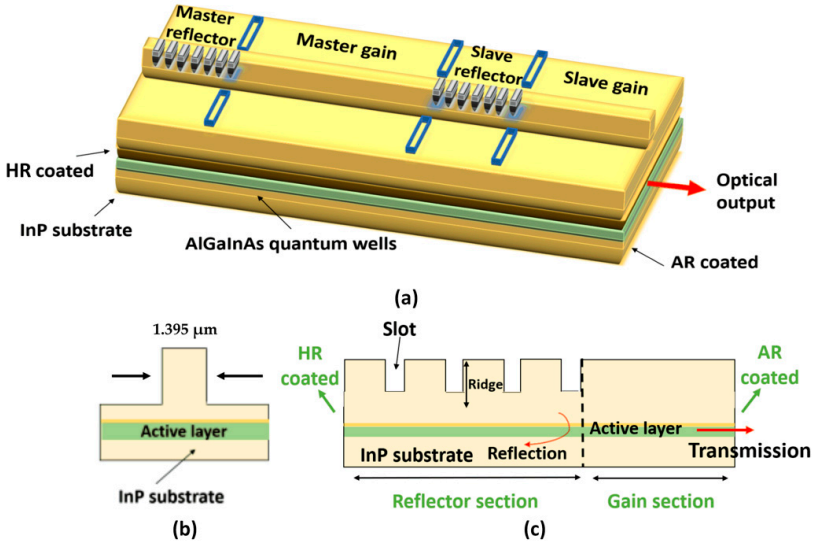

Figure 1. (**a**) InP multi-section photonic integrated circuit (PIC) 3D schematic diagram; (**b**) 2D side view of the waveguide structure; and (**c**) 2D two section single laser waveguide structure.

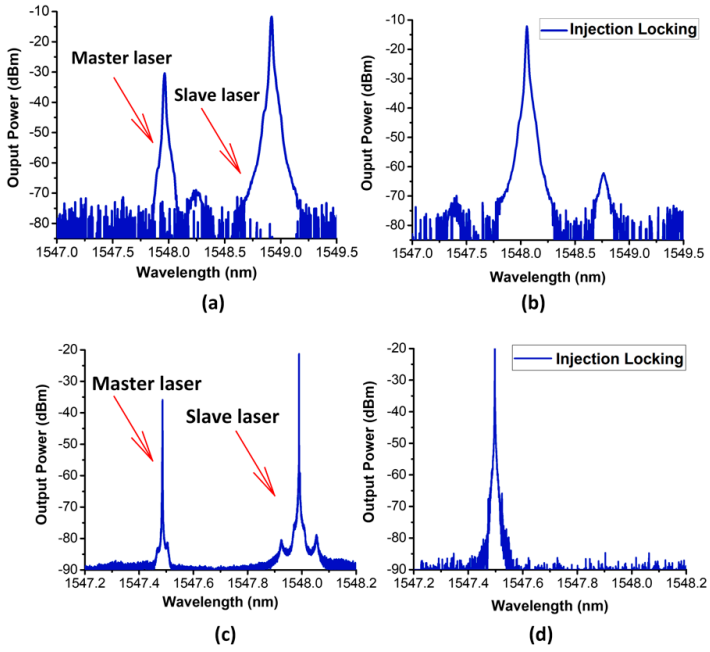

Figure 2. (**a**) Continuous-wave (CW) spectrum of the master (biased at 35 mA) and slave (biased at 90 mA) lasers operating in single-mode operation; (**b**) PIC output spectrum after OIL is achieved (bias point 1 in Table 1). A 20 dB optical attenuator is placed at the input of the OSA for both optical spectra. (OSA resolution: 20 pm); (**c**) CW spectrum of the master (biased at 40 mA) and slave (biased at 60 mA) lasers operating in single-mode operation and (**d**) PIC output spectrum after OIL is achieved (bias point 2 in Table 1). A 30 dB optical attenuator is placed at the input of the OSA for both optical spectra, (OSA resolution: 0.04 pm).

Table 1. Bias points for injection locking spectra.

Section	SG	SR	MG	MR
Bias point 1 (mA)	93.7	65.15	34.67	67.65
Bias point 2 (mA)	65	39	54	49

The independence of the two spectral modes and the fact that each of the distinct modes originates from a different laser can be confirmed by calculating the wavelength/frequency difference between the cavity modes. Figure 3a,b show the optical spectra of the two distinct lasers measured using a 20 pm high-resolution OSA (Yokagawa AQ6370). Figure 3a shows the CW optical spectrum of the slave laser (SG = 80 mA, SR = 40 mA) taken when the master laser is turned off (MG,MR = 0 mA). Within the given OSA resolution, the obtained free spectral range (FSR) between the modes extents between 85 and 100 GHz. A 85 GHz frequency difference corresponds to a cavity length of 550 µm, which is approximately equal to the length of the slave laser cavity (SG + SR sections) (570 µm). This is calculated using the following formula: $\Delta\nu = c/2nL$, where $\Delta\nu$ is the FSR, with n a refractive index of 3.2 and a cavity length of L. Figure 3b shows the CW optical spectrum of the master laser (MG = 80 mA, MR = 8 mA), when the slave laser is biased at transparency (SG = 20 mA, SR = 5 mA). Here, the mode spacing is around 50 GHz, thus corresponding to a cavity length of 937 µm—approximately equal to the master laser cavity length (MG + MR sections) (927 µm). These results confirm the possibility of achieving independent single mode emission from each distinct laser. The master laser emission wavelength can then be controlled, by varying its bias and tuned to achieve OIL. The obtained results are summarized in Table 2 below for clarity.

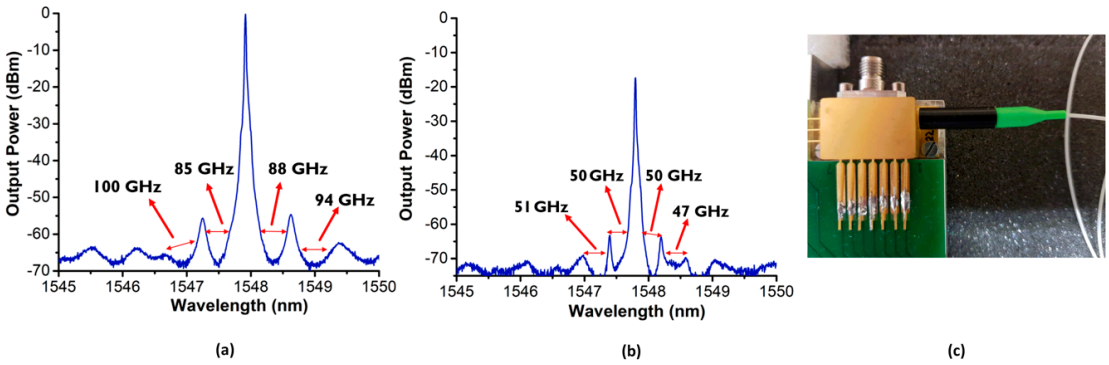

Figure 3. (**a**) Slave laser CW spectrum (master laser is turned off); (**b**) Master laser CW spectrum (slave laser is biased at transparency). A 20 dB optical attenuator is placed at the input of the OSA for both optical spectra. and (**c**) 7-pin high speed butterfly package of the multi-section PIC.

Table 2. Cavity length correpondence calculation.

Bias Condition	Frequency Spacing	Calculated Cavity Length	Actual Cavity Length
SG = 80 mA, SR = 40 mA, MG,MR = 0 mA	85 GHz	550 µm	SG + SR = 570 µm
SG = 20 mA, SR = 5 mA, MG = 80 mA, MR = 8 mA	50 GHz	937 µm	MG + MR = 927 µm

The PIC can be operated in an OIL regime by fine-tuning the DC bias applied to the different sections. However, it is important to note that under certain bias points, the PIC portrays operation in a coupled cavity regime. This is mainly because the two lasers share the same optical waveguide, which leads to multi-cavity effects. Furthermore, the presence of finite electrical isolation between the different sections suggests the presence of some current leakage between the device sections. This current leakage, even if small, would mean that variation of the bias applied to one section would affect the other section.

For ease of use and experimentation, the PIC is encased in a 7-pin, temperature-controlled, fibre pigtailed high-speed butterfly package, as shown in Figure 3c. A radio frequency (RF) connector, attached to the SG section, allows for high-speed modulation of the device. This package contains a thermoelectric cooler (TEC) to accurately control the device temperature to ensure stable operation of the device and a 10 kΩ thermistor for temperature reading to confirm the temperature stability. The device temperature is maintained at 20 °C throughout all the experimental measurements performed in this paper to ensure that uniformity and consistency are maintained.

3. Static Characterization

Static characterization can divulge information on stable regions of operation and provide quantitative details on important parameters that determine the capability of the device to be used in next generation short-reach optical networks. These parameters are the emission wavelength, RIN, SMSR, output optical power, and optical linewidth. First, the dependency of the output spectra of the PIC on the bias values of the different sections is investigated, using contour plots.

3.1. DC Characterization of the PIC

Here, we start by applying different combinations of DC bias to the four different sections of the PIC using a multi-channel current controller (LDC-3900). The light emitted by the SG section is recorded using an OSA with a spectral resolution of 20 pm.

Several important parameters can be extracted from the optical spectrum, such as the main mode peak power and emission wavelength, as well as the SMSR. Both the current controller and the OSA are driven by an automated Python script, which varies the bias of a specific section at each sweep. Contour plots are generated for both the slave and master lasers.

Figure 4a–c show the main mode peak power, SMSR, and main mode emission wavelength of the slave laser, as a function of the SG and SR bias currents, respectively. For this test, the master laser is turned off (MG and MR biased at 0 mA). Figure 4d–f show the same parameters for the master laser, as a function of MG and MR bias currents. Here, the slave laser is biased just above transparency (SG = 10 mA, SR = 5 mA) to minimize any interaction between master and slave lasers. The SG and MG sections biases are varied from 0 to 150 mA, while the SR and MR section biases are varied from 0 to 100 mA as per the safe operating conditions of the PIC. From Figure 4a, it can be observed that the SG has an average threshold of around 32 mA, when the SR is biased over 20 mA. This threshold value decreases with the increase of the SR bias. In addition, it can be noted that lasing from the SR section can be observed when the SG is at least biased at 30 mA and the SR is biased at least 65 mA. From Figure 4a,b, it can be seen that for single-mode operation (high SMSR > 40 dB), the peak power of the slave reaches a maximum of 9 dBm. The SMSR contour plot in Figure 4b allows one to identify the bias currents that result in a high SMSR (dark red regions) as well as the currents at which the device shows multi-mode behaviour (blue and cyan regions). The latter has been confirmed by observing a bi-modal operation of the slave laser on the OSA. A high SMSR of around 55~60 dB can be achieved for several bias points. Figure 4c shows the emission wavelength of the slave laser main mode. From the plot, it can be observed that by varying the currents, the wavelength of the slave laser can be tuned gradually over ~2 nm, before a mode hop occurs (marked by an abrupt change in colour). The multi-coloured region on the left of the plot corresponds to the noise in the OSA, since for those currents the laser is biased below the threshold. The gradual variation in the emission wavelength (between the mode hops) is caused by temperature changes due to the Joule effect [19] occurring with the increase in the bias of the SG and SR sections. When the temperature increases, the central emission wavelength of the laser experiences a redshift [20]. This dependence is more obvious for the SG section than for the SR, due to lack of a grating in the SG section.

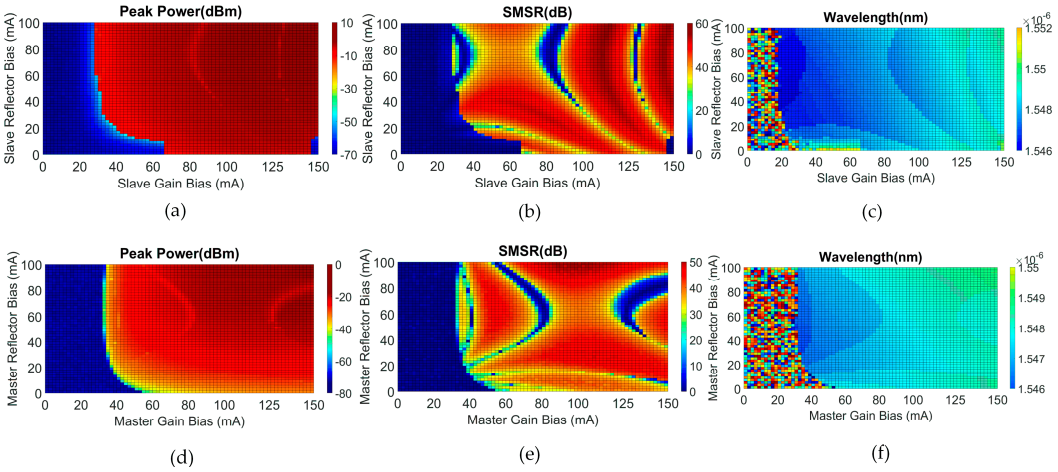

Figure 4. Contour plots of varying SG, SR bias currents and observing the following parameters: (**a**) slave peak power of the main mode; (**b**) slave SMSR of the output modes of the PIC; (**c**) slave emission wavelength of the main mode; and varying MG, MR bias currents and observing the following parameters: (**d**) master peak power of the main mode; (**e**) master SMSR of the output modes of the PIC and (**f**) master emission wavelength of the main mode.

Master laser characterization shows that the MG has an average threshold of ~45 mA (around 13 mA higher than SG threshold), when the MR is biased higher than 20 mA, as depicted in Figure 4d. The higher threshold value can be attributed to the fact that the master laser has a longer cavity length. Again, it can be seen that the MR lases only when the MG is biased above 40 mA, as illustrated in the same figure. The master laser SMSR contour plot shown in Figure 4e manifests a comparable behavior with that of the slave laser. By careful control of the biases applied to the two sections of the master laser, a SMSR as high as 50 dB can be achieved.

Figure 4f shows the capability of the master laser wavelength to be gradually tuned over ~1.5 nm, through variation of the bias currents. Mode hopping only takes place for a few points of bias currents where we experience low SMSR. On the whole, it can be concluded from the different contour plots that a similar behaviour of the master laser and slave laser is obtained with slight variations of power, SMSR, and emission wavelengths values. These plots provide a good understanding of the device behaviour and a means to determine the optimum bias points that will ensure a single-mode emission with high SMSR and high output power. Having carried out a detailed characterization of the operating bias currents, we then chose optimum ones to carry out measurements of the optical linewidth and RIN.

3.2. Linewidth and RIN Measurements

With the ever-growing demand for bandwidth, future short-reach networks may need to employ coherent modulation schemes that combine both amplitude and phase modulation to increase the amount of data being transferred through an optical network [21]. In such networks employing higher-order modulation formats, optical transmitter parameters such as the linewidth and RIN play an important role in determining the overall system performance. Hence, the linewidth and RIN are characterized to determine the suitability of the proposed PIC to be used in next-generation coherent short-reach networks.

Characterization results show that applying injection from the master laser into the slave laser improves important parameters such as linewidth and RIN, as long as the device is operating at single-mode regime. Many operating OIL bias points listed in Table 3 could be chosen as highlighted earlier. However, for the sake of clarity, only two of these optimum operating points' (bias points 1, 2 listed in Table 3) linewidth results are highlighted in this paper.

Table 3. Bias points for linewidth measurements.

Section	SG	SR	MG	MR
Bias point 1 (mA)	45	58	112	74
Bias point 2 (mA)	97.9	50.98	98	92
Bias point 3 (mA)	99.93	99.64	56.73	54.83
Bias point 4 (mA)	93.7	65.18	34.67	68.96
Bias point 5(mA)	100.18	69.7	45.35	85.15

The delayed self-heterodyne (DSH) technique [22], with a resolution of 50 kHz, is used to measure the linewidth of the device at different operating points. The linewidth measurements results are presented in Figure 5a,b where the PIC is biased at two different optimum operating points "bias points 1, 2" as indicated in Table 3 below for Figure 5a,b, respectively. The blue trace shows the master laser linewidth on its own, the red trace shows the slave laser linewidth on its own, and the green trace shows the linewidth of the slave laser injection-locked by the master laser.

Table 4. Bias points for RIN measurements.

Section	SG	SR	MG	MR
Bias point 1 (mA)	45	58	112	74
Bias point 2 (mA)	100.16	69.7	45.3	87.19

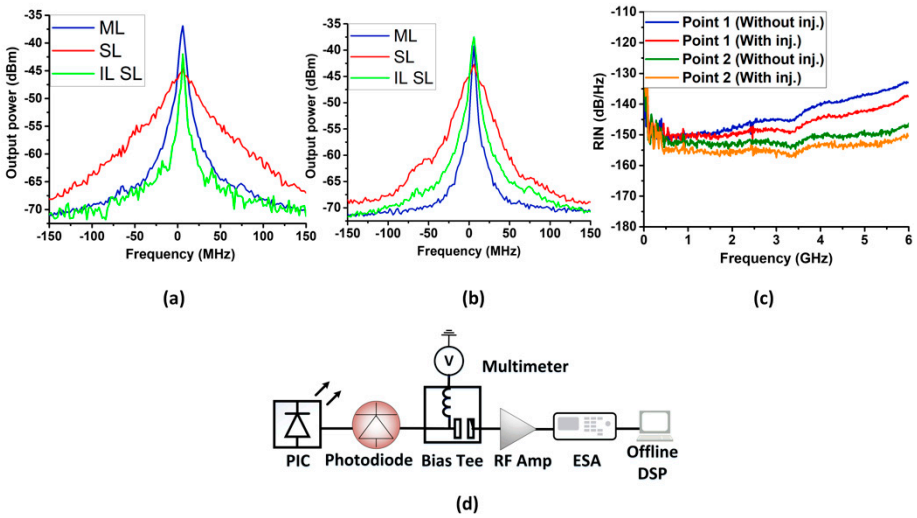

Figure 5. (**a**) Electrical spectra of the measured linewidth of master laser (ML), slave laser (SL) and injection-locked slave laser (IL SL) the master laser for bias point 1 in Table 3; (**b**) same for bias point 2 in Table 3; (**c**) RIN values for bias points 1,2 in Table 4 with (red, orange) and without injection (blue, green) and (**d**) RIN measurement setup diagram.

From Figure 5a, it is evident that the free-running slave laser has a large linewidth of 8 MHz, which can be ascribed to its short cavity. The long cavity master laser at bias current of 112 mA has a much lower linewidth of 2 MHz. The optical linewidth of the slave laser can be significantly reduced by employing OIL from the lower linewidth master laser. OIL is achieved at bias point 1 listed in Table 3. As OIL allows for the transfer of the phase noise characteristics from the master to the slave laser [23], the linewidth of the latter is reduced to 2 MHz, as shown in Figure 5a. Similar behaviour is shown in Figure 5b, where again the lower linewidth of the master laser (2.7 MHz) was imposed into the slave laser through OIL. This results in decreasing the slave laser large linewidth from 5 MHz to 2.7 MHz (the device is biased at "bias point 2" listed in Table 3). It is important to note that this PIC is a proof of concept device and the potential of further improvement exists. We anticipate that there will

be a second generation of this device, which could be expected to give improved performance and linewidth results. However, the reduced linewidth as a result of the injection can still enable the device to be used with higher order modulation formats at high baud rates [24].

RIN is another important parameter of an optical transmitter, quantifying the intensity fluctuations of the laser output power [25]. High RIN values (>−120 dB/Hz) can be a limiting factor for the usage of a laser in DCNs, especially ones employing multi-level intensity modulation schemes such as PAM 4/8 [26]. Moreover, it can also have a negative effect on other modulation schemes such as orthogonal frequency division multiplexing (OFDM) and discrete multi-tone transmission (DMT) [27] that may be used to directly modulate the laser transmitter. The RIN characterization of the proposed four-section device has been carried out using an experimental set-up depicted in Figure 5d [28]. The optical emission of the DC biased device is detected by a 20 GHz high-speed photodetector (Thorlabs DXM20AF). The output of the photodiode is then connected to a bias tee (through the RF + DC terminal) to separate the DC and the AC components of the generated photocurrent. The DC port of the bias tee is connected to a multimeter, while the AC output is connected to an electrical amplifier, followed by a 6 GHz electrical spectrum analyser (ESA) (R&S FSL6). The latter is used to capture the AC component, resulting from optical power fluctuations of the laser. The RIN is computed based on both the AC component obtained from the ESA and the DC component obtained from the multimeter, using the equation below:

$$\mathrm{RIN} = \frac{\Delta P_E}{P_{EO}}, \tag{1}$$

where P_{EO} is the average electrical power (DC component), while ΔP_E is the overall noise of the laser (AC component). The latter consists of three different components: the noise of the laser itself (N_L), the thermal (N_{th}), and shot (N_q) noise. Figure 5c shows the obtained RIN values for bias points "1 and 2" listed in Table 4 below with and without injection.

The obtained averaged value of RIN (DC to 6 GHz) of "bias point 1" in Table 4 without injection (blue trace) (both MG and MR biases are set to zero) is −143.4 dB/Hz. Turning the master laser sections on (MG = 112 mA, MR = 74 mA) (red trace) decreases the average RIN to −146.1 dB/Hz. The reduction of RIN value for the injected case can be attributed to the reduction of cavity gain by the injected signal. This reduction also causes the carrier density to deplete, resulting in a decrease of the overall spontaneous emission rate, which in turn reduces the overall RIN of the PIC [29]. A similar reduction in the RIN value is shown also for "bias point 2" listed in Table 4 in the same figure. The RIN value obtained without injection (green trace) is −151.6 dB/Hz. This value decreases to −154.3 dB/Hz by turning the master laser on (MG = 45 mA, MR = 87 mA) and applying optical injection (orange trace). The obtained results demonstrate that the integrated device has a relatively low RIN value qualifying it as a potential candidate to be used in direct intensity modulated short-reach communication networks [30].

Having concluded the static characterization of the PIC, we further investigate the dynamic performance of the PIC to determine its usefulness as a directly modulated transmitter for DCNs.

4. Dynamic Characterization

External modulation is one of the most popular techniques of modulating data onto an optical signal and offers several advantages, such as high bandwidth (stemming from the modulation bandwidth of the external modulator used) and the possibility to generate complex modulation formats. Currently available external intensity modulators can achieve high modulation bandwidths >40 GHz [31]. However, the external modulator suffers from several disadvantages, such as high insertion loss (which needs to be compensated using optical amplifiers), bias drift, and polarization dependence. These features act as obstacles in using external modulation in cost-sensitive applications, such as DCNs and short-reach networks. Direct modulation, on the other hand, is a simple and cost-effective technique, where data modulation is accomplished simply by adding the information

signal to the bias current of the laser [32]. The main drawbacks here are the limited laser bandwidth and the frequency chirp. The first one restricts the maximum modulation data rate, while the second leads to a broadening of the optical spectrum, which in conjunction with fiber dispersion, limits the transmission distance [33].

OIL can be implemented to overcome both of these drawbacks, thus extending the data rates and the transmission distances achievable in systems employing direct modulation. Previous reports have shown that external injection can enhance the intrinsic modulation bandwidth of the laser up to about three times [10,13]. There are also some studies on how injection locking can be used to significantly reduce the chirp of a directly modulated laser [15,34].

4.1. Modulation Response of the PIC

We start by measuring the small-signal frequency response of the slave laser using the setup in Figure 6a (dotted and continuous red lines). Two measurement scenarios are implemented: with and without optical injection from the master laser. We referred back to our original static characterization and chose two optimum operating points, "bias points 1 and 2", in Table 5 below. We turned the master laser off to realize the first scenario (without injection) and simply turned the master laser on with the bias values stated in Table 5 to realize the second scenario (with injection).

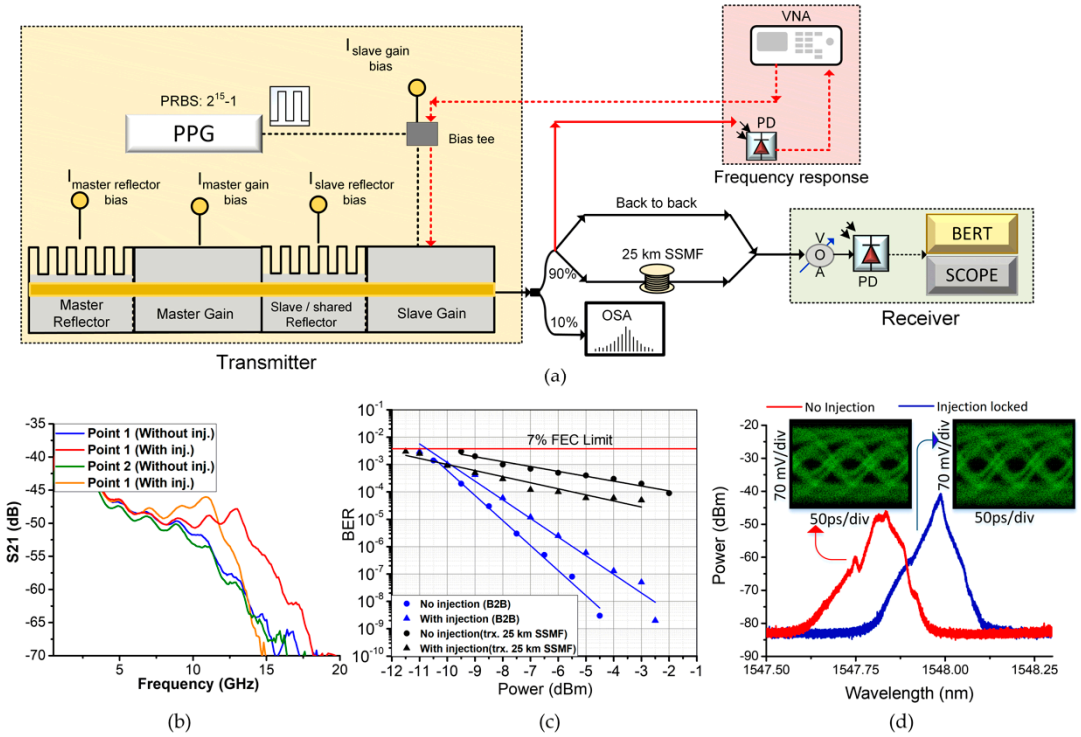

Figure 6. (**a**) Schematic setup diagram of frequency response measurements (red wire connections), short-reach transmission system (black wire connections); solid lines: optical connections, dashed lines: electrical connections; (**b**) frequency response of the slave laser two bias points of the PIC listed in Table 5 without (blue, green) and with (red, orange) injection; (**c**) BER results for back to back (B2B) (blue) and 25 km SSMF transmission distances (black) with and without injection; (**d**) optical spectra of the PIC under modulation with injection (blue) and without injection (red); inset: obtained eye diagrams after 25 km SSMF transmission and 0.5 dBm received optical power.

Table 5. Bias points for frequency response measurements.

Section	SG	SR	MG	MR
Bias point 1 (mA)	100.18	69.7	45.35	85.15
Bias point 2 (mA)	98.68	56.15	65.62	87.56

For this measurement, a 50 GHz network analyzer (HP 8517B) is used to directly modulate the SG section of the device. The frequency of the modulated RF signal is swept from 0.05 to 20 GHz. The optical output of the PIC is split using a 90:10 coupler, where the 90% branch is detected by a 20 GHz photodiode (DSC30S) and then sent back to port 2 of the network analyzer. The other 10% branch is used to monitor the optical spectrum (ensuring single-mode operation) of the device. The measured S_{21} parameter (i.e., the frequency response) of the slave laser is shown in Figure 6b.

The measurement is first carried out for the free-running slave laser biased at "bias point 1" in Table 5 without injection (MG,MR = 0) (blue trace) and subsequently for the optical injection case (red trace). The figure shows that by employing OIL, the 3 dB modulation bandwidth of the slave can be increased from 9.5 to 14 GHz (45% enhancement). The same measurement is conducted for "bias point 2" in Table 5. Slave laser without injection (green trace) shows a 3 dB modulation bandwidth of 9.2 GHz. Injection from the master laser improves the modulation bandwidth to 12.1 GHz. The improvement as a result of injection from the master laser enables higher direct modulation rates of the device as well as improves the linearity of the slave laser frequency response (much flatter frequency response over the given data bandwidth).

4.2. Direct Data Modulation and On-Off Keying (OOK) Transmission

Next, we carry out direct data modulation of the SG section of the PIC with a 10.7 Gb/s OOK data signal to investigate the potential of usage of the PIC as a transmitter in a short reach network. The experimental setup used is shown in Figure 6a (black wire connections). A pulse pattern generator (PPG) is used to generate a 10.7 Gb/s pseudo random bit sequence (PRBS) with a length of $2^{15}-1$. The data signal is combined with a DC bias of 72.8 mA using an internal bias-tee within the device package. The optical output of the device is split using a 90%-10% coupler. The 10% path is connected to a 20 MHz high-resolution OSA, while the 90% path is launched into a 20 GHz PIN photodiode (DSC30S) either B2B or after transmission over 25 km of SSMF. A variable optical attenuator (VOA) is used to vary the received optical power. The photodiode output is connected either to a digital sampling oscilloscope, to generate eye diagrams, or to an error detector, to measure the bit error rate (BER) of the system.

BER results as a function of the received optical power are presented in Figure 6c. The measurements are taken for both the cases when the master laser was turned off (circles) and on (triangles). For the B2B transmission, the injected case has a power penalty of 2 dB with respect to the non-injected one at BER $= 4 \times 10^{-9}$. This penalty can be attributed to the fact that the optical injection reduces the threshold current of a laser, resulting in a degraded extinction ratio [35]. However, after transmission over 25 km of SSMF, the optically injected laser performs significantly better. The received optical power required to achieve the FEC limit for the injection case is 2 dB lower than that without injection. This can be attributed to a reduction of the chirp due to the applied OIL [36]. For both cases, a BER below the hard decision (7% overhead) forward error correction (FEC) limit (BER $= 3.8 \times 10^{-3}$) is achieved. The optical spectra recorded using a 0.04 pm resolution OSA (APEX AP2433B) in Figure 6d further verify the reduction in frequency chirp, where the OIL case is represented by the blue line and the non-injected case by the red line. It can be seen that the spectral width of the modulated laser without OIL is significantly broader than when the master laser is turned on. The interplay between the fiber chromatic dispersion and this large spectral width (due to higher value of chirp) causes pulse spreading, leading to intersymbol interference and resulting in a degraded performance (worse BER). The insets in Figure 6d show the recorded eye diagrams at a received optical

power of 0.5 dBm for both cases. The reduced eye-opening for the laser without injection is visible and validates the results of the BER measurements.

5. Conclusions

A novel PIC structure that can be employed as a low-cost optical transmitter system in the next generation short-reach networks is presented. The device consists of two lasers integrated in a master-slave configuration, where the master laser injects light into the cavity of the slave laser to improve its spectral characteristics. A set of static and dynamic characterizations are conducted on the PIC to analyze several important parameters of consideration for next-generation short-reach optical networks, including optical linewidth, RIN, and frequency response. Furthermore, the enhancements that OIL can provide to these parameters are presented. The reduction in linewidth of the PIC from 8 to 2 MHz due to OIL is demonstrated. Moreover, the RIN measurements show averaged RIN values as low as −154.3 dB/Hz, which allows the use of the device with multi-level modulation formats. Furthermore, it shows the reduction of RIN by applying OIL from the master laser. On the dynamic characterization part, the PIC shows a 4.5 GHz (45%) improvement in the modulation bandwidth under injection. Transmission performance of the injected case shows a 2 dB improvement in the minimum optical power required to achieve a bit error rate of 3.8×10^{-3} (hard decision forward error correction limit) as a result of reduction in chirp by OIL.

These improved spectral characteristics, achieved due to the OIL, are accompanied by the attractive features of photonic integration, qualifying the multi-section PIC to be used in next-generation optical short-reach networks. In the future, we will aim to improve the PIC design to further reduce the linewidth of the master laser as well as to increase the control of the power injected from the master into the slave laser. This will result in further enhancements of the device spectral characteristics and performance.

Author Contributions: Conceptualization, M.N.H., A.K.-A., P.L., and P.M.A.; Methodology, M.N.H., A.K.-A., and P.M.A.; validation, M.N.H., A.K.-A., M.D.G.P., G.J., and P.D.L.; formal analysis, M.N.H., G.J., and A.K.-A.; investigation, M.N.H., A.K.-A., P.D.L., G.J., P.L., and M.D.G.P.; resources, P.M.A., A.K.-A., and M.D.G.P.; data curation, M.N.H.; writing—original draft preparation, M.N.H. and P.D.L.; writing—review and editing, M.N.H., P.L., A.K.-A., M.D.G.P., P.D.L., and P.M.A.; visualization, M.N.H., A.K.-A., P.L., and P.M.A.; supervision, P.M.A., P.L. and A.K.-A.; project administration, P.M.A., P.L., and A.K.-A.; funding acquisition, P.M.A. All authors have read and agreed to the published version of the manuscript.

Funding: This research was funded by Science Foundation of Ireland's (SFI) career development award (15/CDA/3640), SFI 17/IFB/5385, and Regional Development Fund (13/RC/2077).

Acknowledgments: We would like to acknowledge the support given by the technical officers (Robert Clare, Liam Meany) in the school of Electronic Engineering, Dublin City University.

Conflicts of Interest: The authors declare no conflict of interest.

References

1. Cisco Global Cloud Index: Forecast and Methodology 2016–2021. Available online: https://www.cisco.com/c/en/us/solutions/collateral/service-provider/global-cloud-index-gci/white-paper-c11-738085.html (accessed on 10 September 2019).
2. Coldren, L.A.; Corzine, S.W. *Diode Lasers and Photonic Integrated Circuits*; John Wiley and Sons: New York, NY, USA, 1995.
3. Cheng, Q.; Bahadori, M.; Glick, M.; Rumley, S.; Bergman, K. Recent advances in optical technologies for data centers: A review. *Optica* **2018**, *5*, 1354–1370. [CrossRef]
4. Bettotti, P. Hybrid Materials for Integrated Photonics. *Adv. Optics Hindawi Publ. Corp* **2014**, 2356–6817. [CrossRef]
5. Gordon, R. Fabry-Perot semiconductor laser injection locking. *IEEE J. Quantum Electron.* **2006**, *42*, 353–356. [CrossRef]
6. Lin, C.; Mengel, F. Reduction of frequency chirping and dynamic linewidth in high-speed directly modulated semiconductor lasers by injection locking. *Electron. Lett.* **1984**, *20*, 1073–1075. [CrossRef]

7. Chrostowski, L.; Chang, C.H.; Chang-Hasnain, C.J. Reduction of relative intensity noise and improvement of spur-free dynamic range of an injection locked VCSEL. In Proceedings of the 16th Annual Meeting of the IEEE Lasers and Electro-Optics Society, Tucson, AZ, USA, 27–28 October 2003. [CrossRef]
8. Iwashita, K.; Nakagawa, K. Suppression of mode partition noise by laser diode light injection. *IEEE Trans. Microw. Theory Tech.* **1982**, *10*, 1657–1662. [CrossRef]
9. Lau, E.K.; Wong L., J.; Wu, M.C. Enhanced Modulation Characteristics of Optical Injection-Locked Lasers: A Tutorial. *IEEE J. Sel. Topics Quantum Electron.* **2009**, *15*, 618–633. [CrossRef]
10. Barry, L.P.; Anandarajah, P.; Kaszubowska, A. Optical pulse generation at frequencies up to 20 GHz using external-injection seeding of a gain-switched commercial Fabry-Perot laser. *IEEE Photonics Tech. Lett.* **2001**, *13*, 1014–1016. [CrossRef]
11. Simpson, T.B.; Liu, J.M. Enhanced modulation bandwidth in injection-locked semiconductor lasers. *IEEE Photonics Tech. Lett.* **1997**, *9*, 1322–1324. [CrossRef]
12. Paoli, T.L.; Ripper, J.E. Direct modulation of semiconductor lasers. *Proc. IEEE* **1970**, *58*, 1457–1465. [CrossRef]
13. Anandarajah, P.M.; Latkowski, S.; Browning, C.; Zhou, R.; O'Carroll, J.; Phelan, R.; Kelly, B.; O'Gorman, J.; Barry, L.P. Integrated Two-Section Discrete Mode Laser. *IEEE Photonics J.* **2012**, *4*, 2085–2094. [CrossRef]
14. O'Carroll, J.; Anandarajah, P.M.; Zhou, R.; Phelan, R.; Kelly, B.; O'Gorman, J.; Barry, L.P. Transmission over 50 km using a directly modulated integrated two-section discrete mode laser at 1550 nm. In Proceedings of the CLEO EUROPE/IQEC, Munich, Germany, 12–16 May 2013. [CrossRef]
15. Yabre, G. Effect of relatively strong light injection on the chirp-to-power ratio and the 3 dB bandwidth of directly modulated semiconductor lasers. *J. Lightwave Tech.* **1996**, *14*, 2367–2373. [CrossRef]
16. Pascual, M.D.G.; Vujicic, V.; Braddell, J.; Smyth, F.; Anandarajah, P.M.; Barry, L.P. InP photonic integrated externally injected gain switched optical frequency comb. *Opt. Lett.* **2017**, *42*, 555–558. [CrossRef] [PubMed]
17. Herbert, C.; Jones, D.; Kaszubowska-Anandarajah, A.; Kelly, B.; Rensing, M.; O'Carroll, J.; Phelan, R.; Anandarajah, P.M.; Perry, P.; Barry, L.P.; et al. Discrete mode lasers for communication applications. *IET Optoelectron.* **2009**, *3*, 1–17. [CrossRef]
18. Lu, Q.; Guo, W.; Byrne, D.; Donegan, J.F. Design of Slotted Single-Mode Lasers Suitable for Photonic Integration. *IEEE Photon. Tech. Lett.* **2010**, *22*, 787–789. [CrossRef]
19. Pipe, K.P.; Ram, R.J.; Shakouri, A. The physics of heat transport in semiconductor lasers. In Proceedings of the IEEE 18th International Semiconductor Laser Conference, Garmisch, Germany, 29 September–3 October 2002. [CrossRef]
20. Mahdi, M.S.; Ali, A.H.; Alaa, H.; Hussein, M.H. Heat Effects on Data Transmission by Laser Diode and Light Emitted Diode for High Frequency Optical Communication Systems. *J. Nanosci. Technol.* **2016**, *2*, 126–129.
21. Kikuchi, K. Coherent transmission systems. In Proceedings of the 34th European Conference on Optical Communication (ECOC), Brussels, Belgium, 21–25 September 2008. [CrossRef]
22. Richter, L.; Mandelberg, H.; Kruger, M.; McGrath, P. Linewidth determination from self-heterodyne measurements with subcoherence delay times. *IEEE J. Quantum Electron.* **1986**, *22*, 2070–2074. [CrossRef]
23. Tang, C.L.; Statz, H. Phase-Locking of Laser Oscillators by Injected Signal. *J. Appl. Phys.* **1967**, 38. [CrossRef]
24. Dhawan, D.; Gupta, N. Investigation of Tolerable Laser Linewidth for Different Modulation Formats in CO-OFDM Systems. *Opt. Photonics J.* **2017**, *7*, 92–100. [CrossRef]
25. Pillai, R.; Garmire, E.; Menendez-Valdes, P. Relative intensity noise of laser-diode arrays. *IEEE Photonics Tech. Lett.* **1991**, *3*, 968–970. [CrossRef]
26. Vujicic, V.; Anthur, A.P.; Saljoghei, A.; Panapakkam, V.; Zhou, R.; Gaimard, Q.; Merghem, K.; Lelarge, F.; Ramdane, A.; Barry, L.P. Mitigation of relative intensity noise of quantum dash mode-locked lasers for PAM4 based optical interconnects using encoding techniques. *Opt. Express* **2017**, *25*, 20–29. [CrossRef]
27. Miaofeng, L.; Rong, H.; Jinsong, X.; Qi, Y.; Xi, X.; Cai, L.; Xiang, L.; Shaohua, Y. Cost-effective coherent PON using silicon Mach-Zehnder modulator and digital carrier regeneration. *Opt. Express* **2015**, *23*, 19799–19805. [CrossRef]
28. Relative Intensity Noise of Distributed Feedback Lasers, Application note. Available online: https://www.eagleyard.com/fileadmin/downloads/documents/eyP_App_Note_RIN__1-6.pdf (accessed on 22 September 2019).
29. Jin, X.; Chuang, S.L. Relative intensity noise characteristics of injection-locked semiconductor lasers. *Appl. Phys. Lett.* **2000**, *77*, 1250–1252. [CrossRef]
30. Lee, H.; Moon, J.; Mun, S.; Choi, K.; Lee, C. Decision Threshold Control Method for the Optical Receiver of a WDM-PON. *IEEE/OSA J. Opt. Comm. Netw.* **2010**, *2*, 381–388. [CrossRef]

31. Wiberg, A.; Perez-Millan, P.; Andres, M.V.; Andrekson, P.A.; Hedekvist, P.O. Fiber-optic 40-GHz mm-wave link with 2.5-Gb/s data transmission. *IEEE Photon. Technol. Lett.* **2005**, *17*, 1938–1940. [CrossRef]
32. Kobayashi, S.; Yamamoto, Y.; Ito, M.; Kimura, T. Direct frequency modulation in AlGaAs semiconductor lasers. *IEEE J. Quantum Electro.* **1982**, *18*, 582–595. [CrossRef]
33. Maher, R.; Shi, K.; Anandarajah, P.M.; Kaszubowska, A.; Barry, L.P.; Yu, Y. Novel Frequency Chirp Compensation Scheme for Directly Modulated SG DBR Tunable Lasers. *IEEE Phot. Technol. Lett.* **2009**, *21*, 340–342. [CrossRef]
34. Okajima, Y.; Hwang, S.K.; Liu, J.M. Experimental observation of chirp reduction in bandwidth-enhanced semiconductor lasers subject to strong optical injection. *Opt. Comm.* **2003**, *219*, 357–364. [CrossRef]
35. Nguyen, Q.T.; Besnard, P.; Bramerie, L.; Shen, A.; Garreau, A.; Vaudel, O.; Kazmierski, C.; Duan, G.-H.; Simon, J.-C. Using optical injection of Fabry-Perot lasers for high-speed access in optical telecommunications. In Proceedings of the SPIE Photonics Europe, Brussels, Belgium, 12–16 April 2010. [CrossRef]
36. Hwang, S.K.; Tian, J.M. Chirp reduction in directly-modulated semiconductor lasers subject to external optical injection. In Proceedings of the IEEE LEOS Annual Meeting Conference, Sydney, Australia, 22–28 October 2005. [CrossRef]

© 2020 by the authors. Licensee MDPI, Basel, Switzerland. This article is an open access article distributed under the terms and conditions of the Creative Commons Attribution (CC BY) license (http://creativecommons.org/licenses/by/4.0/).